PNAS RESEARCH ARTICLE | MICROBIOLOGY
BIOPHYSICS AND COMPUTATIONAL BIOLOGY OPEN ACCESS

Distantly related bacteria share a rigid proteome allocation strategy with flexible enzyme kinetics

Manlu Zhu[a,1], Matteo Mori[b,1], Terence Hwa[b,2], and Xiongfeng Dai[a,2]

Affiliations are included on p. 8.

Contributed by Terence Hwa; received December 27, 2024; accepted March 21, 2025; reviewed by Vickery L. Arcus and Seppe Kuehn

Bacteria are known to allocate their proteomes according to how fast they grow, and the allocation strategies employed strongly affect bacterial adaptation to different environments. Much of what is currently known about proteome allocation is based on extensive studies of the model organism *Escherichia coli*. It is not clear how much of *E. coli*'s proteome allocation strategy is applicable to other species, particularly since different species can grow at vastly different rates even in the same growth condition. In this study, we investigate differences in nutrient-dependent proteome allocation programs adopted by several distantly related bacterial species, including *Vibrio natriegens*, one of the fastest-growing bacteria known. Extensive quantitative proteome characterization across conditions reveals an invariant allocation program in response to changing nutrients despite systemic, species-specific differences in enzyme kinetics. This invariant program is not organized according to the growth rate but is based on a common internal metric of nutrient quality after scaling away species-specific differences in enzyme kinetics, with the faster species behaving as if it is growing under a higher temperature. The flexibility of enzyme kinetics and the rigidity of proteome allocation programs across species defy common notions of evolvability and resource optimization. Our results suggest the existence of a blueprint of proteome allocation shared by diverse bacterial species, with implications on common underlying regulatory strategies. Further knowledge on the existence and organization of such phylogeny-transcending relations also promises to simplify the bottom–up description and understanding of bacterial behaviors in ecological communities.

bacterial growth | resource allocation | proteomics | bacterial phylogeny | enzyme kinetics

Significance

Different bacterial species can grow at different rates in their respective optimal growth conditions. What makes some grow faster than others? Of particular interest is *Vibrio natriegens*, one of the fastest growing bacterial species known, and a desirable chassis for numerous synthetic biology applications. This work shows that *V. natriegens* adapts its proteome in different growth conditions much like well-studied model bacteria such as *Escherichia coli* and *Bacillus subtilis*; it grows faster because its enzymes are faster, as if it were growing at higher temperatures. The quantitative, comparative proteomic analysis presented here reveals a high degree of similarity between proteomes of species far apart in phylogeny, raising the question of the underlying physiological constraints driving this convergent evolutionary process.

Growth control is an essential determinant of bacterial fitness. In recent years, systems and quantitative biology approaches have revealed fundamental roles of proteome resource allocation in governing bacterial growth in response to different environmental conditions and genetic perturbations (1–5). In the meantime, the recent explosion of studies in microbial ecology (6–10) demands an understanding of similarities and differences in proteome allocation strategies for different bacterial species in a community. Unlike comparative genomics, interspecies proteome comparisons are complicated by the interplay between growth conditions and protein allocation (11–16). Current knowledge, based largely on studies of the model bacterium *Escherichia coli*, is ingrained on the notion that the proteome is allocated to different functions in accordance with the growth rate (4, 5, 16–19). But different species often grow at wildly different rates, even on the same nutrients and at the same temperatures (20–26). Therefore, it is not obvious a priori how the proteome of different species should be compared.

In this study, we take on this challenge and establish a methodology for quantitative interspecies proteome comparison. We focus on three exemplary species: the very distantly related model bacteria *E. coli* and *Bacillus subtilis* (27, 28) and *Vibrio natriegens*, which is relatively closely related to *E. coli* but has a superfast growth characteristics across nutrient conditions (29, 30). By performing extensive experiments quantifying their proteomes, along with additional kinetic characterization across a range of nutrient conditions and at different temperatures, we arrive at a number of simple, quantitative relations that transcend their phylogenetic relation. These surprising results challenge common notions about the rigidity and flexibility of the underlying evolutionary processes connecting the different species.

Results

Constraints in Proteome Allocation for Fast-Growing Bacteria. Extensive physiological studies in the past decades have established stringent requirements on resource allocation for model bacteria such as *E. coli* (Ec) and *B. subtilis* (Bs), particularly on the allocation

Author contributions: M.Z., M.M., T.H., and X.D. designed research; M.Z., M.M., and X.D. performed research; M.Z. and X.D. contributed new reagents/analytic tools; M.Z., M.M., T.H., and X.D. analyzed data; and M.Z., M.M., T.H., and X.D. wrote the paper.

Reviewers: V.L.A., University of Waikato; and S.K., University of Chicago.

The authors declare no competing interest.

[1]M.Z. and M.M. contributed equally to this work.

[2]To whom correspondence may be addressed. Email: hwa@ucsd.edu or daixiongfeng@ccnu.edu.cn.

This article contains supporting information online at https://www.pnas.org/lookup/suppl/doi:10.1073/pnas.2427091122/-/DCSupplemental.

Published April 29, 2025.

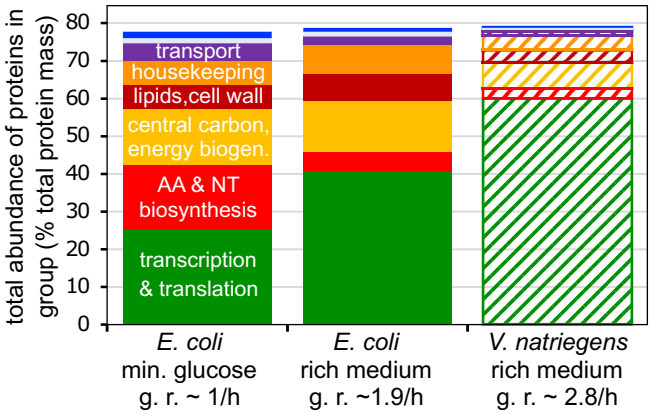

Fig. 1. Protein abundances in minimal and rich medium. Abundances of proteins belonging to various functional groups for *E. coli* grown in glucose minimal medium (*Left* bar) and rich medium (*Middle* bar). Abundances are measured in percent of total protein mass. These data are computed based on the protein mass abundance measurement obtained from mass spectrometry analysis (34), using functional groups defined in Dataset S3. The shaded bar on the right depicts a hypothetical proteome for *V. natriegens* wherein the allocation for gene expression machineries is 50% more than that of Ec (thus from 40% to 60% of the proteome), and the allocation for the other functional groups are reduced to half those *of E. coli* (thus with the total of the groups reduced from ~40% to ~20% of the proteome).

of the proteome to ribosomes, which increases linearly with the growth rate (4, 12, 31–33). In Ec, translation machineries comprise over 20% of the proteome by mass in glucose minimal medium and over 40% in rich medium (16, 34) (green bars, Fig. 1). Most of this increase is compensated by reduction in the amount of enzymes for amino acid and nucleotide biosynthesis (red bars, Fig. 1), which are not needed in rich medium. In contrast, other functional groups change little between these two media.

In this context, it is interesting to examine the proteome allocation strategy by *Vibrio natriegens* (Vn), one of the fastest-growing microbes (30, 35) which grows >50% faster than Ec and Bs when growing in the same nutrient and temperature (Fig. 2 *A* and *B*). The fast growth potential has made Vn an attractive chassis for synthetic biology applications (35, 36), while also raising basic questions on molecular ingredients enabling rapid bacterial growth. Because Vn grows substantially faster than Ec in rich medium, one might expect the allocation to translation machineries to be further increased, if the linear relation between ribosome content and growth rate known for Ec and Bs can be extended to Vn. But if this is so, then allocation to other functional groups needed at fast growth would be severely squeezed, reducing from 60% of the proteome for Ec to 40% of the proteome for Vn (shaded bar in Fig. 1). This would imply Vn's enzymes for the other cellular processes to be twice as efficient as those of Ec, i.e., either Vn enzymes are 50% faster if the processes are enzyme-limited in Ec, or otherwise, Ec enzymes are expressed at levels that are 50% above what are needed to support growth, and Vn reduced the excess expression. Alternatively (or in addition), the widely accepted linear relation of ribosome content with growth rate cannot be applied when comparing across organisms. As we will see, investigating how Vn allocates its proteome to achieve its supercharged growth led us to a surprisingly simple resource allocation strategy that transcends phylogeny and is applicable to organisms regardless of the actual growth rates.

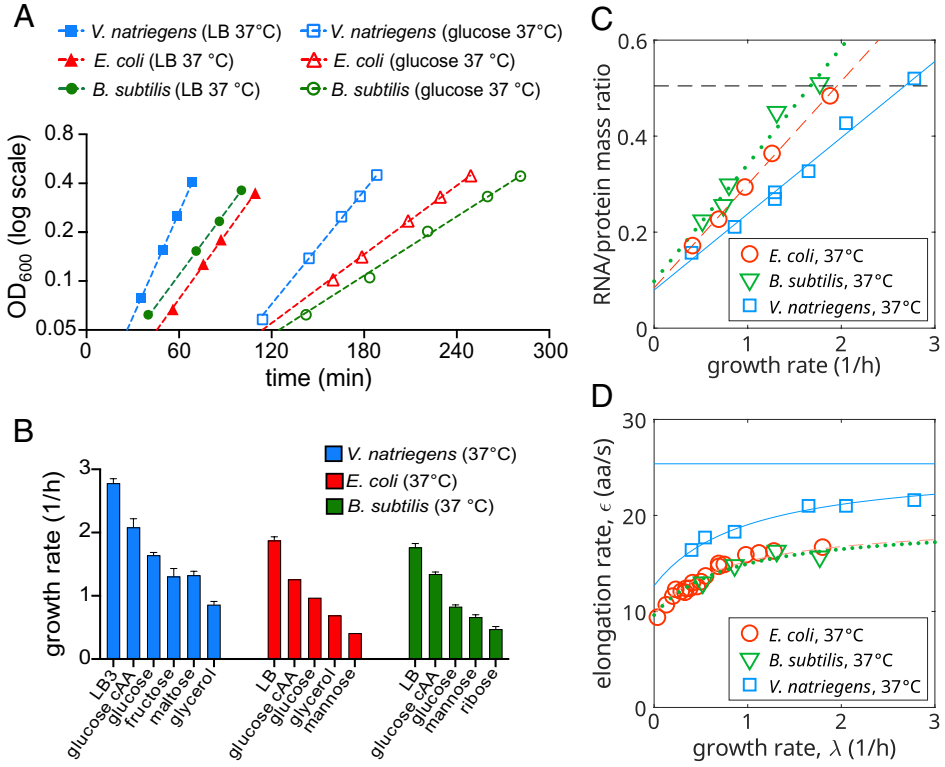

Fig. 2. Ribosome abundances and kinetics for three bacterial species across nutrients and temperatures. (*A*) Growth curves (optical density vs time) of Ec, Bs, and Vn in LB and in glucose minimal medium, all at 37 °C. (*B*) Growth rates of these three species in a variety of rich and minimal media; see *SI Appendix*, Tables S1 and S2 for strain and medium details; all minimal media for Bs are supplemented with 1 mM glutamate to suppress sporulation. (*C*) Linear correlation between RNA–protein ratio and growth rate (R-line) for cultures of Ec, Bs, and Vn growing exponentially at 37 °C in different nutrients. Colored lines are the best linear fits. The horizontal black line indicates the average R/*P* value for the three species in LB media. R/P data of *E. coli* in four growth media including glu cAA, cAA, glucose, mannose, and glycerol media) are taken from a previous study (37). (*D*) Translational elongation rate (ER) measured for each species grown in various nutrients at 37 °C. The ER data for Ec are taken from a previous study (37). Colored curves show the best one-parameter fit to the expected hyperbolic form, *SI Appendix*, Eq. **S1.4** in *Note* S1.

Ribosome Elongates Faster in Vn as if Temperature Increased. We first quantified the RNA–protein (R/P) ratio, a proxy of the ribosome content (38), for the three organisms growing in various nutrient sources supporting a range of growth rates (*SI Appendix*, Tables S1 and S2). For each species, the R/P ratio follows a linear relation with the growth rate (λ), referred to as the R-line (Fig. 2*C*). However, Vn's R-line exhibits a reduced slope, indicating that Vn reaches a larger growth rate than Ec and Bs for the same ribosome content (e.g., dashed horizontal lines in Fig. 2*C*). Since Vn is getting faster growth from the same ribosome content as Ec and Bs, this suggests that the translational elongation rate (ER, denoted by ε) is faster in Vn. This is confirmed by direct measurement (37) (*SI Appendix*, Figs. S1 and S2) for cells grown in rich and minimal medium (Fig. 2*D*).

This behavior of changing the growth rate by changing ER while keeping the ribosome content unchanged is reminiscent of Ec's response to temperature changes (26, 39). Extending the physiological study of these three species to different temperatures, we indeed found that the R-line of all three species flattens as the temperature is increased (*SI Appendix*, Fig. S3). We measured growth rates for the three species in rich media across a range of temperatures. The growth rate is well known to satisfy an approximate exponential dependence with the inverse temperature, consistently with the Arrhenius law of reaction kinetics (26); using a four-parameter model (*SI Appendix*, *Note* S4), we extracted the Arrhenius activation energies, as well as maximal and optimal temperatures, and the maximal growth rate; fits are shown as solid lines in Fig. 3*A* and results are summarized in Fig. 3*B*. All species had similar activation energies, $E_a \sim 15$ kcal/mol, suggesting similar activation energies for growth-limiting metabolic processes such as protein synthesis. Comparing Ec and Bs, we note that they have similar growth at low temperature (below 30 °C), but Bs can withstand higher temperatures. Instead, Vn grows faster than both Ec and Bs in the same temperature range. For example, Vn has the same maximum growth as Bs, but displays a shift in the optimal and maximal temperatures of about 10 °C (Fig. 3*B*).

From the temperature dependences of the growth rate in rich media, we observed that Vn at 30 °C has a growth rate close to that of Ec at 37 °C (blue box in Fig. 3*A*), while Vn at 37 °C grows similarly to Bs at 43 °C (purple box). We thus investigated whether the abundance and activity of ribosomes was also similar for these two pairs of species and temperatures. Strikingly, both the R-line and ER of Vn grown at 30 °C are comparable to those of Ec grown at 37 °C (Fig. 3 *C* and *D*), and those of Vn grown at 37 °C are comparable to those of Bs grown at 43 °C (Fig. 3 *E* and *F*). Thus, it appears that Vn grows as if experiencing an effective temperature higher than that of Ec and Bs.

Ribosome Elongation Rate Sets the Rate of Cell Growth. The notion that Vn resembles Ec or Bs grown at higher temperatures can be quantitatively formulated in terms of the fastest ER attainable by a species at a given temperature. This quantity, denoted as ε^* and taken empirically to be the ER for cells grown in the medium giving the fastest growth rate (LB in this case), is plotted in Fig. 4*A* for each species at each temperature characterized, and in Fig. 4*B* as a function of the inverse temperature. The plots show that an upward shift of ε^* by Vn is equivalent to a shift to higher temperatures by a given organism (red arrows). This equivalence between the change of organism shift and shift in temperature is extended to growth rates: since the growth rate in LB, λ^*, is given by the product of ER and ribosome abundance in LB, and the latter is nearly the same for all three species at all temperatures (Fig. 2*C* and *SI Appendix*, Fig. S3), it follows that λ^* is proportional to ε^* for all three species and temperatures (Fig. 4*C*). The linear relation in Fig. 4*C* is the first example of phylogeny-transcending relations that we will encounter in this study.

Phylogeny-Transcending Relation Between Growth Rate and Ribosome Content. Importantly, ε^* also governs the growth dynamics in other nutrient conditions beyond rich medium. First, the flatness (i.e., inverse of the slope) of the R-lines shown in *SI Appendix*, Fig. S3 is seen to be proportional to the corresponding ε^* for each species and temperature studied (Fig. 4*D*). This linear relation, in quantitative agreement with the model of proteome allocation developed for Ec by Wu et al (40) (reviewed in *SI Appendix*, *Notes* S1 and S2), is followed also by Bs and Vn and thus represents another phylogeny-transcending relation, which now covers a spectrum of growth conditions. Further, since the R-lines of all three organisms (and at all temperatures) exhibit similar y-intercepts (Fig. 2*C* and *SI Appendix*, Fig. S3), it follows that all the R/P data collapse onto a single line upon scaling the growth rate by ε^* (Fig. 4*E*).

A similar data collapse is seen for the elongation rates when they are also normalized by ε^* and plotted against the scaled growth rate (Fig. 4*F*). The hyperbolic relation between $\varepsilon/\varepsilon^*$ and λ/ε^* that emerges (solid line, Fig. 4*F*) can be understood as a consequence of the Michaelis relation between ER and the R/P ratio, established empirically for Ec (see ref. 37, reviewed in *SI Appendix*, *Note* S2), and apparently also applicable to Bs and Vn. This phylogeny-transcending relation, can be reexpressed in the following suggestive form,

$$\lambda = \varepsilon^* \cdot h\left(\varepsilon/\varepsilon^*\right), \qquad [1]$$

where the form of the function h is derived in *SI Appendix*, Eq. **S1.11** in *Note* S1. Eq. **1** has a very important biological interpretation: first, the overall scale of the growth rate of an organism at a given temperature is set by ε^*; we refer to this as the organism's "growth potential". Second, the ratio $\varepsilon/\varepsilon^*$, which reflects the saturation of the ribosome's translational activity (henceforth referred to as "ribosome saturation"), provides an *internal metric* of the external nutrient condition. For Ec, ribosome saturation is simply related to the level of the alarmone ppGpp (40); see *SI Appendix*, *Note* S2. The data collapse shows that the growth rates of the distantly related Bs and Vn are governed by the same form; hence Eq. **1** is a phylogeny-transcending relation that describes the nutrient dependence of the growth rate of each species at each temperature through the species-invariant function h. Eq. **1** also provides a concrete biological interpretation to the collapse of R/P data by the scaled growth rate λ/ε^* (Fig. 4*E*): the linear dependence of R/P on λ/ε^* can be expressed as a linear dependence on $h(\varepsilon/\varepsilon^*)$, reflecting a species-invariant dependence of R/P on nutrient conditions through ribosome saturation.

Comparative Proteomics Across Species. As cell growth requires many proteins beyond ribosomes (especially in minimal medium), we next examined the allocation of the entire proteome for these species using quantitative mass spectrometry (see *SI Appendix*, *Supplementary Methods*; see also ref. 16), to see whether other functionalities might be governed by similar phylogeny-transcending relations. A proteomic analysis was performed to obtain the absolute (mass) abundances of up to ~2,000 proteins each for Ec, Bs, and Vn using xTop analysis (*SI Appendix*, *Note* S3 and Fig. S4, and refs. 16 and 34), each across five nutrient conditions and at two temperatures (*SI Appendix*, Table S3). The resulting abundances

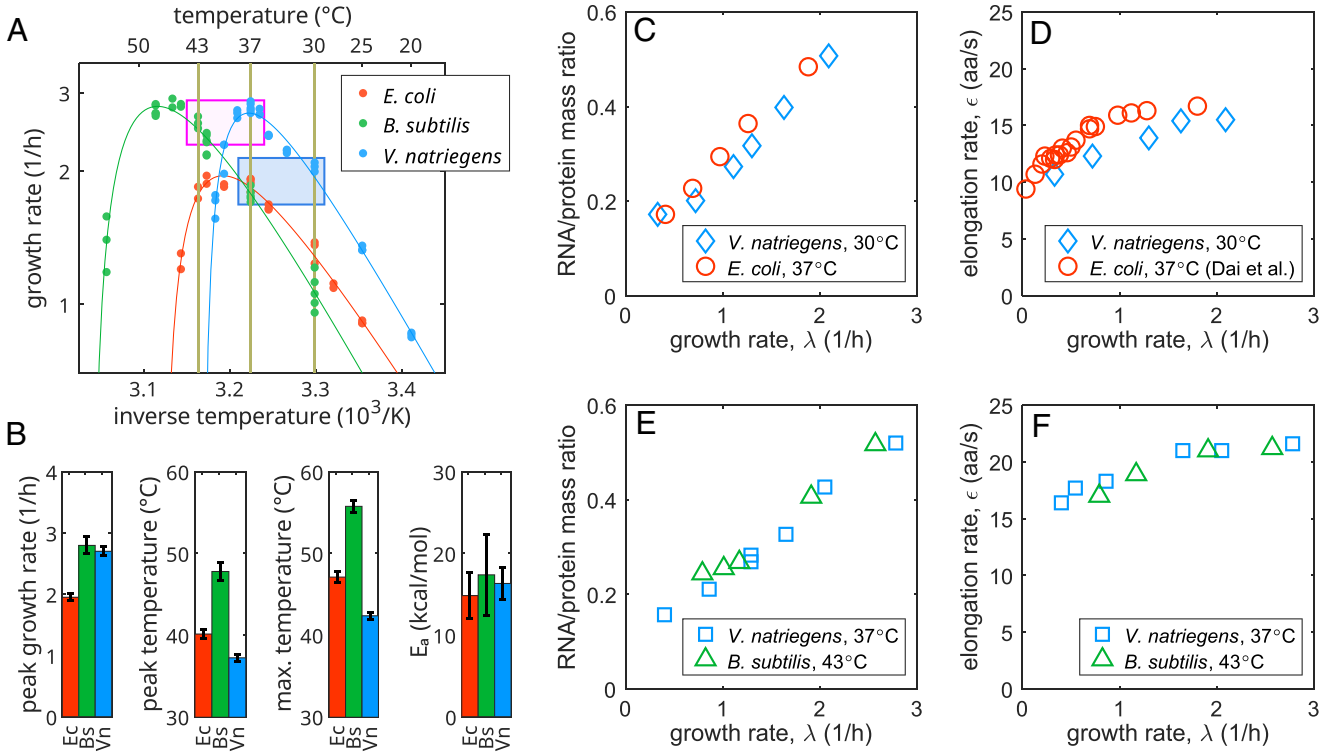

Fig. 3. Ribosomal characteristics at different temperatures. (*A*) The three species Ec, Bs, Vn were each grown in LB for a range of temperatures. The growth rates exhibited a clear Arrhenius region, i.e. a linear dependence on the inverse temperature. The data were fitted to a four-parameter model (*SI Appendix, Note* S4) in order to extract the peak growth rate with the corresponding peak growth temperature, the maximum permissible temperature, and the activation energy of the Arrhenius region; the fit results are shown in panel (*B*) (error bars represent 95% CI). All species had similar activation energies $E_a \sim 15$ kcal/mol. Ec and Bs have similar growth rates at low temperature, but Bs growth extended ~10 °C further *E. coli*'s, indicating that it tolerates high temperature better, being otherwise kinetically similar to Ec. Instead, Bs and Vn growth had similar peak growth rates, but both the peak growth temperature and the maximum permissible temperature were shifted by ~10 °C, indicating that Vn grows faster than Ec and Bs at 37 °C as if it were growing at a higher effective temperature. For Ec (red), 37 °C lies at the high-temperature end of the Arrhenius regime; at higher temperatures (through 42 °C), the level of heat stress proteins is elevated even if growth rate does not decrease (16). For Bs (green), growth rate reaches its peak at ~45 °C. We characterized the species at 43 °C, at which the growth rate is similar to that of Vn at 37 °C (pink box), to avoid triggering heat shock responses. For Vn (blue), growth rate nearly peaks at 37 °C. We also characterized Vn at 30 °C where its growth rate is similar to that of Ec and Bs at 37 °C (blue box). To complete the comparisons, we also characterized Ec at 30 °C. (*C*) RNA–protein ratio and (*D*) the elongation rate of Ec and Bs at 37 °C and of Vn at 30 °C. (*E*) RNA–protein ratio and (*F*) the elongation rate of Vn at 37 °C and of Bs at 43 °C.

(Dataset S1) agree well with those estimated previously from ribosome profiling (13, 17) for the same three species grown in rich medium; see *SI Appendix*, Fig. S4*C*.

Abundances of individual proteins are nearly unchanged for an organism grown at different temperatures in the same nutrient condition (*SI Appendix*, Fig. S5 *A–F*) despite ~50% faster growth by Vn, well exceeding similarity in different nutrient conditions at the same temperature (*SI Appendix*, Fig. S5 *G–I*). The abundance of homologous proteins (obtained via pairwise BLAST comparison, Dataset S2) is also similar between Ec/Bs/Vn grown in the same conditions (*SI Appendix*, Fig. S6 *A–D*). However, the similarity in abundance is dependent on the degree of homology imposed in ortholog identification (*SI Appendix*, Fig. S6*E*), suggesting that the simple pairwise comparison may be polluted by paralogs with distinct functions; the varied phylogenetic distances between the species pairs further complicates the comparison, with homologues in Ec and Vn showing higher similarity scores than homologues between Bs and one of the other species.

Phylogeny-Transcending Allocation of Major Protein Functional Groups. To overcome uncertainties associated with ortholog identification, we assigned proteins to 66 functional groups which are further organized into three tiers of coarse graining (Dataset S3). We then followed how the abundances of these groups changed across nutrient conditions for each organism. First, we show the results at the coarsest level for three supergroups: transcription and translation (Fig. 5*A*), amino acid and nucleotide biosynthesis (Fig. 5*B*), and central carbon metabolism and energy biogenesis (Fig. 5*C*), which together account for ~50% of the proteome by mass in each organism (Fig. 5*D*). Plotting the fractional mass abundance ϕ_i of each protein group i against the scaled growth rate (λ/ϵ^*), we found the abundances of these protein groups to be highly overlapping for the three species (Fig. 5 *A–C*), similar to the collapse of the R/P data (Fig. 4*E*). For example, the allocation to transcription and translation in LB (ϕ_{tt}^*) is maximal at ~40% for all three species (Fig. 5*A*), and the allocation to biosynthesis in the fastest-growing minimal medium ($\phi_{syn}^\dagger$) is maximal at ~20%, dropping in LB (ϕ_{syn}^*) to a basal level of ~5% for these species (Fig. 5*B*).

The data collapse seen in these plots indicates that the abundance of each group i, ϕ_i, is a unique function of the scaled growth rate λ/ϵ^*, which, as discussed above, reflects a common internal metric of nutrient conditions, the ribosome saturation ϵ/ϵ^* (Eq. **1**). Using Eq. **1** to interpret the scaled growth rate, i.e., $\lambda/\epsilon^* = h(\epsilon/\epsilon^*)$, the data collapse here can be expressed succinctly as

$$\phi_i = f_i(\epsilon/\epsilon^*), \qquad [2]$$

with the abundance of each group i having a species-invariant dependence f_i on nutrient conditions (through the ribosome saturation ϵ/ϵ^*).

This general pattern of quantitative similarity in proteome allocation across these species persists at a finer (intermediate) level of protein grouping (*SI Appendix*, Fig. S7). For example, we see

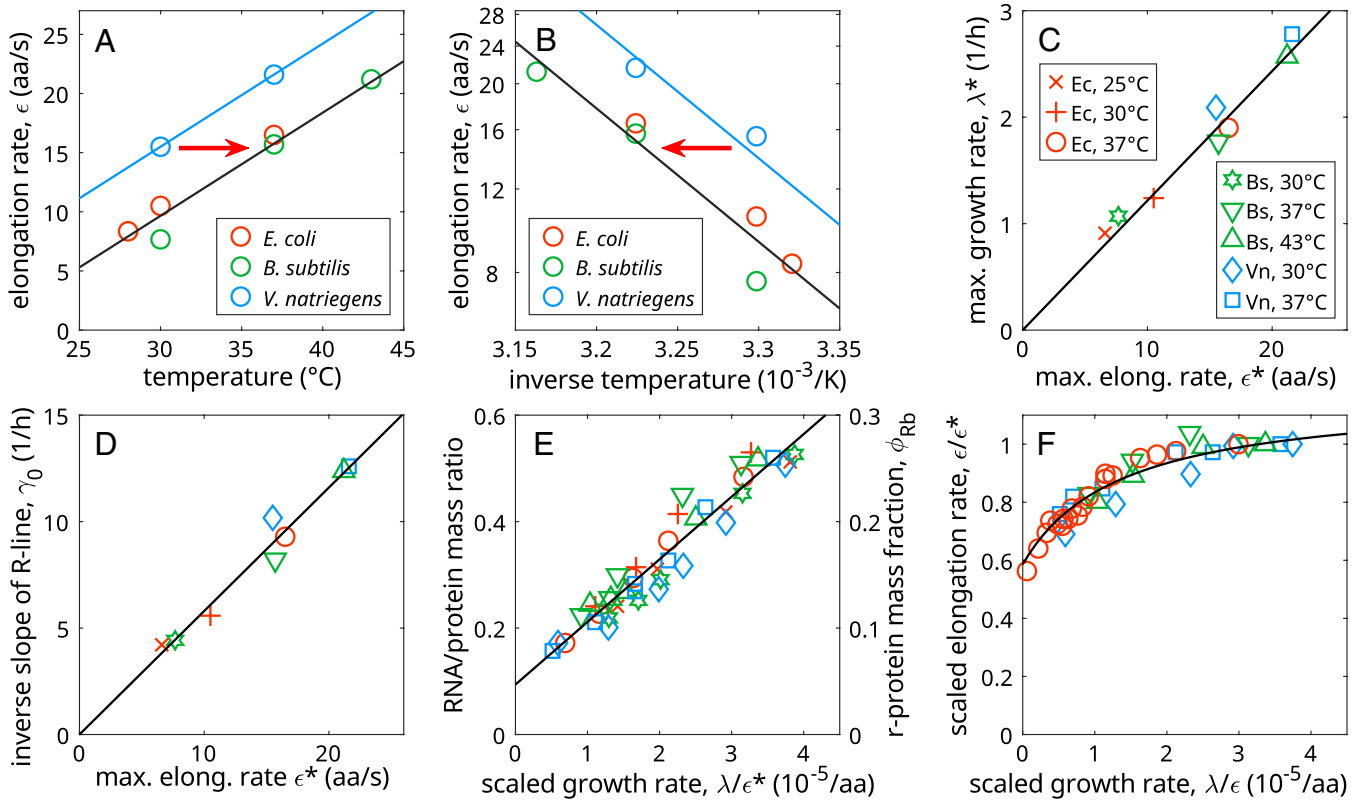

Fig. 4. Phylogeny-transcending relations linking growth rates, elongation rates, and ribosome abundances in different growth conditions. (*A*) ER in rich medium (LB), denoted as ϵ^*, is measured for each species at various temperatures. The blue line, describing the temperature dependence of ϵ^* of Vn, is related to the black line, describing the temperature dependence of ϵ^* of Ec and Bs, by a temperature shift of ~6.7 °C (red arrow) with the same slope. (*B*) Similar to the previous panel, but with elongation rate plotted against inverse temperature in logarithmic scale (Arrhenius plot). The activation energy of the elongation rate obtained from the slope of the lines in this panel (12.9 kcal/mol), is similar to the activation energy found in Fig. 3 *A* and *B*. The lines are related by a vertical shift of 1.5-fold, equivalent to a horizontal shift of $6.3 \cdot 10^{-5} K^{-1}$ (red arrow), corresponding to ~ 5. 7 °C. (*C*) The fastest growth rate (λ^*) of each organism (in LB) attained at each temperature is linearly correlated with the corresponding ER (ϵ^*). (*D*) The values of the inverse-slope of the R-lines (denoted as γ_0), obtained from *SI Appendix*, Fig. S3, are also linearly correlated with ϵ^*. (*E*) The R/P data of the 3 species in all nutrients and temperatures (*SI Appendix*, Fig. S3) are plotted against the scaled growth rate, λ/ϵ^*, whose unit, $h^{-1}/(aa/s)$, is expressed as per aa residue. (*F*) ER data for the three species in all nutrients and temperatures, normalized by ϵ^* for each series and plotted against the scaled growth rate, λ/ϵ^*. The black lines in panels c-f are parameter-free predictions of the proteome allocation model *SI Appendix*, Eqs. **S1.8**, **S1.7**, **S1.9**, and **S1.10**, respectively; see *SI Appendix, Note* S1).

that the abundances of the three components of the translational machinery are highly similar across these organisms (*SI Appendix*, Fig. S7 *A–C*). Enzymes of amino acid biosynthesis (*SI Appendix*, Fig. S7*F*), those involved in central carbon metabolism (*SI Appendix*, Fig. S7 *H–J*), electron transport chain and ATPase (*SI Appendix*, Fig. S7 *L–M*), amino acid recycling (*SI Appendix*, Fig. S7*N*), and fatty acid metabolism (*SI Appendix*, Fig. S7*O*) are also highly similar. Some organism-specific differences can be seen at this level, e.g., Bs allocated less to outer membrane components (*SI Appendix*, Fig. S7*P*) and transport (*SI Appendix*, Fig. S7*Q*), and more to nucleotide biosynthesis (*SI Appendix*, Fig. S7*G*). While the absolute magnitudes of most of these differences are small (1 to 2% of proteome), and they exert little effect on the abundance of the coarse functional groups (Fig. 5 *A–C*), the difference in transport is substantial (~10% for Ec at slow growth while only 2 to 3% for Bs; *SI Appendix*, Fig. S7*Q*). Such reduction in the proteome of Bs at slow growth is mostly compensated by the expression of proteins unique to Bs, such as the nonribosomal peptide synthetases associated to surfactin biosynthesis (*SI Appendix*, Fig. S7*R*) (41). The reduced expression of motility machinery in Vn compared to Ec and Bs also stands out (*SI Appendix*, Fig. S7*S*). For Ec, an increase in motility expression due to active insertion element is well documented for various lab strains (42–44). For Bs, the enhanced motility may be an adaptation to their natural habitat, as many studies have shown enhanced motility function for rhizosphere-associated bacteria including *Bacillus* (45–47). Altogether, the classified proteins account for ~75% of the total protein mass for all three species (*SI Appendix*, Fig. S7*T*).

Individual Pathways Vary More Across Conditions Than Across Species. Another perspective on the interspecies proteome allocation is provided by pairwise quantitative comparisons of the abundances of key protein groups such as amino acid biosynthesis pathways whose functions are the same across organisms; see scatter plots in *SI Appendix*, Fig. S8. These plots appear to show stronger similarity between the proteomes of different species grown in the same nutrient than those of the same species grown in different conditions (e.g. rich and minimal media), again supporting a proteome allocation strategy conserved across species. Below, we confirmed this visual impression with a quantitative analysis across the growth conditions studied.

For the ease of closer comparisons of the abundances of proteins belonging to different functional groups, we show in Fig. 6*A* the abundances of gene expression machinery and main metabolic pathways present in all three species at the finest, level-3 classification (Dataset S3) for all growth conditions studied, with the latter indicated by circles of different filling intensities (Ec: red; Bs: green; Vn: blue). The abundances of proteins belonging to different pathways spanned 2 to 3 orders of magnitude (decreasing from left to right), with the variability across species and conditions increasing for low-abundant pathways. However, each organism often allocated similar amounts of proteins to the same

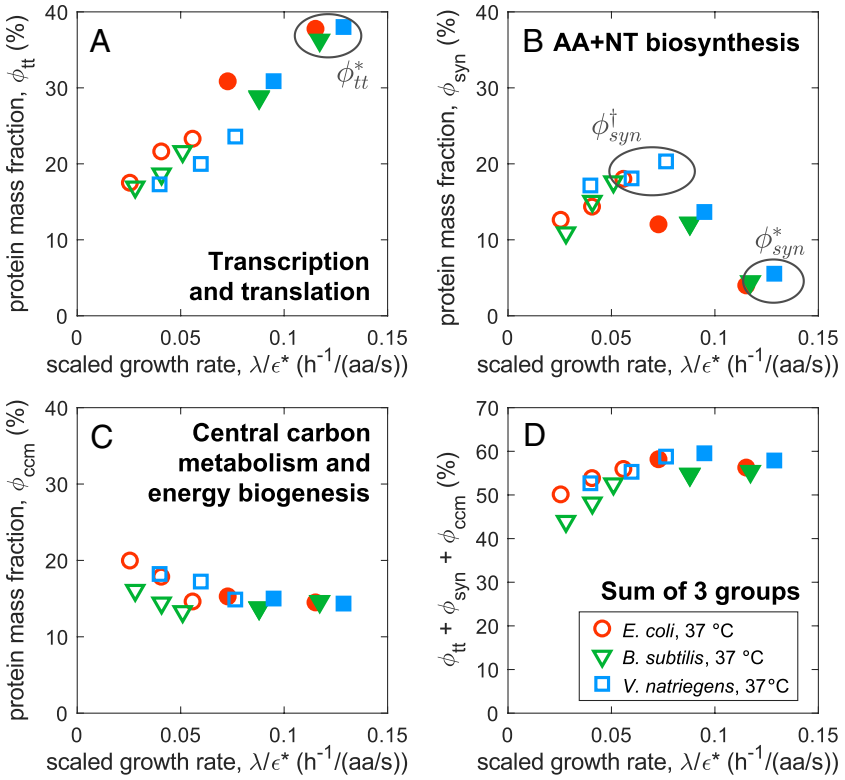

Fig. 5. Growth dependences of protein functional groups for the three species. From the mass spectrometry analysis of *Ec*, *Bs*, and *Vn* at 37 °C, the mass abundances of the individual proteins detected (Dataset S1) are summed for each functional group (defined in Dataset S3) and expressed as a fraction of the total protein mass. The data are plotted against the scaled growth rate λ/ϵ^* for (*A*) the sum of transcriptional and translational machineries, ϕ_{tt}, (*B*) the sum of amino acid and nucleotide biosynthesis, ϕ_{syn}, and (*C*) the sum of central carbon metabolism and energy biogenesis, ϕ_{ccm}, including glycolysis/gluconeogenesis, pentose phosphate pathway, TCA cycle, fermentation to acetate, electron transport chain, and ATP synthase. (*D*) The sum of abundances shown in panels (*A*–*C*). In these plots, the open symbols refer to growth in minimal media and filled symbols refer to rich media (with the right-most symbol of each series being LB). The gray circles in panels *A* and *B* show that despite changes in allocation by each species grown in different nutrients, the allocation across species is conserved, with the maximal allocation to translation and transcription (in rich medium) being $\phi^*_{tt} \approx 40\,\%$, basal allocation for biosynthesis (in rich medium) being $\phi^*_{syn} \approx 5\,\%$, and maximal allocation to biosynthesis (in the fastest minimal medium) being $\phi^\dagger_{syn} \approx 20\,\%$ for each organism.

pathway, even when they exhibited a strong dependence on growth conditions. For example, the amino acid biosynthesis pathways mostly varied within an order of magnitude, between the highly expressed level in minimal medium (open symbols) and the basal level in rich medium (filled symbols). Notable exceptions are the highly reduced expression of the tryptophan biosynthesis pathway by Bs across conditions (attributed to the Bs strain used being a tryptophan auxotroph) (48), and the lower basal levels of a few other pathways (arginine and histidine) by Bs in rich medium.

To make the above comparisons of pathway abundances more systematic and quantitative, we sought to tease apart species-specific effects (s) from effects due to different nutrient conditions (c). To do so, we modeled the log-transformed pathway abundances using a linear mixed model, $\log \phi_{s,c} = \log \phi_0 + x_s + y_c$, with one species-dependent factor x_s and one condition-dependent factor y_c (Fig. 6*B* and *SI Appendix*, *Note* S5 and Fig. S9). These two factors are sufficient to capture the bulk of the variance in the data, with median R^2_{adj} being 0.83 (Fig. 6*C*, black). Neither factor alone fully captured the variance, with the condition-dependent factor giving a much higher median R^2_{adj} (0.55, blue line) than that of the strain-dependent factor (0.10, red line). The condition-dependent factor gives a higher R^2_{adj} in 23 out of 33 cases, significantly larger than one-half (bootstrapped P-value: 0.023). We also quantified the size of the two contributions as the maximum spread in the two factors, R_s and R_c, as illustrated in Fig. 6*B*. Distributions of the effect sizes are shown in Fig. 6*D*: growth conditions (blue) have larger effect sizes compared to the strain-dependent factor in 25/33 cases, significantly more than one-half (bootstrapped P-value: 6×10^{-4}). The median effect size was also larger for the condition-dependent factor versus the species-dependent factor (0.49 versus 0.24). Overall, the analysis showed that the protein amount allocated to the main metabolic pathways depends primarily on the nutrient conditions, rather than on the strains, further reinforcing the global protein allocation patterns observed in Fig. 5 and *SI Appendix*, Fig. S7.

Discussion

A great deal of biology has been learned by comparing the genomes of organisms at various phylogenetic distances (24, 49–51). Comparing the proteomes of organisms is more difficult, even conceptually, because protein abundances depend not only on the phylogeny but also on the conditions the organisms are grown in (11–16). By performing extensive experiments quantifying the proteomes and characterizing the ribosome kinetics of three exemplary bacterial species, each across a range of nutrient conditions and at different temperatures, we arrived at a number of surprising findings.

First, these organisms do not allocate their proteome in the same way according to their growth rate as widely thought. Instead, their proteomes are allocated in accordance to a common internal metric, the degree of saturation of ribosome kinetics, ϵ/ϵ^*. This common internal metric leads to a common allocation

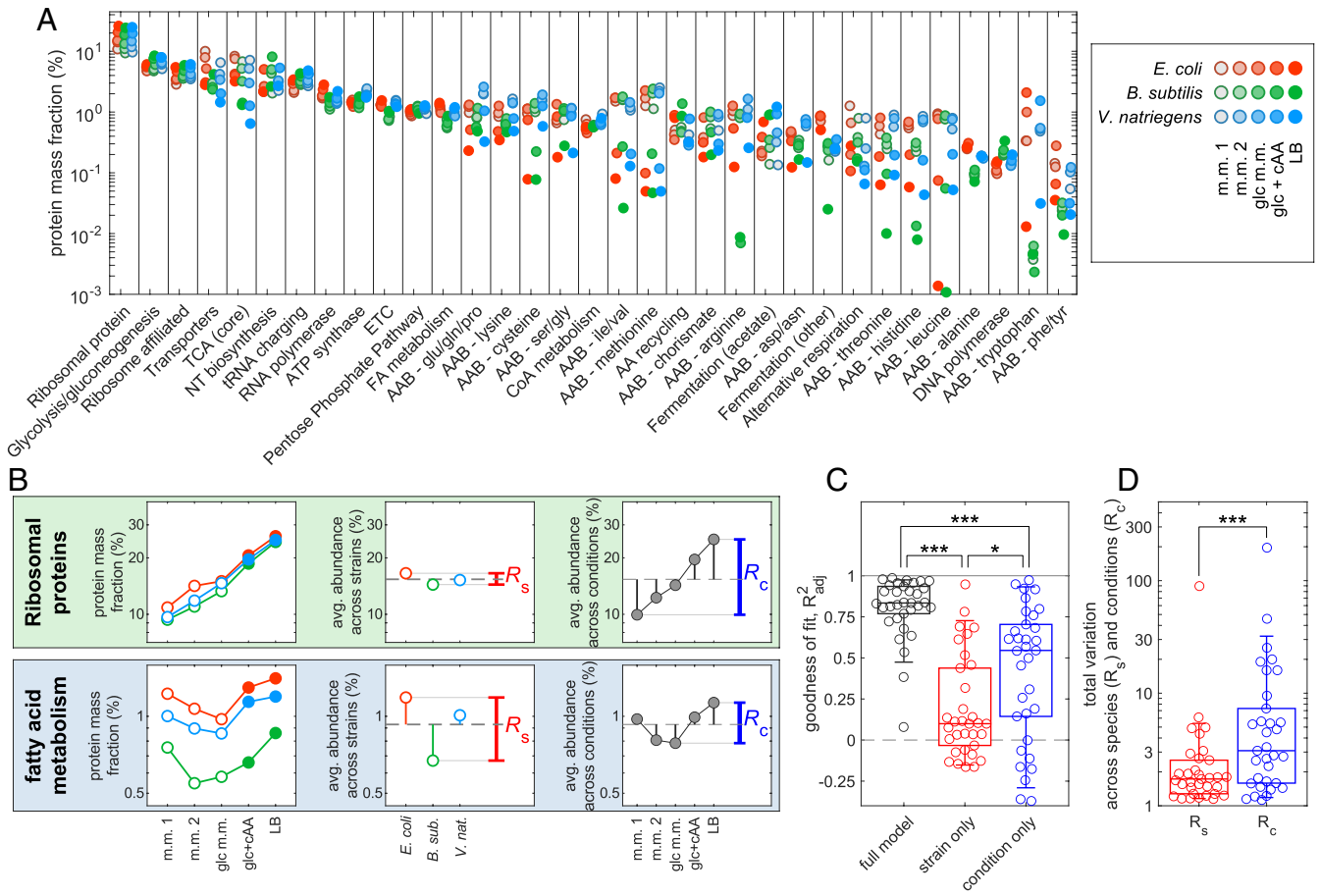

Fig. 6. Decomposition of changes in the allocation for protein groups across conditions and species. (*A*) Abundance of 33 metabolic pathways (up to level-3 classification, see Dataset S3), with different growth conditions indicated by circles of different filling intensities; see legend. (*B*) The *Left* column shows the abundances of two exemplary protein groups (ribosomal proteins, and fatty acid metabolism) plotted across growth conditions for *E. coli* (red), *B. subtilis* (green), and *V. natriegens* (blue); the *Middle* and *Right* columns show the average protein abundances across species and conditions, respectively. In both cases, the protein mass fractions show similar trends across conditions, with large species-dependent offsets in the case of fatty acid biosynthesis. For each protein group, we modeled the log-transformed protein mass fractions ($\log \phi_{s,c}$ for species s in condition c) as linear combinations of an average level $\log \phi_0$, a species-dependent factor x_s, and a condition-dependent factor y_c, i.e. $\log \phi_{s,c} = \log \phi_0 + x_s + y_c$ (*SI Appendix*, *Note* S5); the best fit results for these two protein groups are shown in the *Middle* and *Right* panels, with the average value being represented by the horizontal dashed lines. We further quantified for each protein group the maximum variation across species, R_s, and across conditions, R_c, as indicated in the panel for each protein group. (*C*) Goodness of fit, measured by the adjusted coefficient of determination R^2_{adj}, for each of the protein groups in panel a, using the full model (black), including only the strain-dependent effects (red), or including only the condition-dependent effects (blue). Boxes indicate median and 25% to 75% intervals; whiskers indicate 5% to 95% intervals; asterisks indicate statistical significance (bootstrapped *P*-value; see text). Individual values are shown in *SI Appendix*, Fig. S9. (*D*) Total change in abundance across species (R_s, red), and conditions (R_c, blue) for each protein group. Boxes indicate median and 25% to 75% intervals; whiskers indicate 5% to 95% intervals. Individual values are shown in *SI Appendix*, Fig. S9.

program, or "blueprint," captured by Eq. **2**, conserved down to the level of metabolic pathways, despite the vast phylogenetic distances separating these organisms (27, 28). This finding substantially expands upon a previous report on conservation in the stoichiometry of enzymes of a pathway between distantly related bacteria (13). For *E. coli*, the saturation of ribosome kinetics $\varepsilon/\varepsilon^*$ reflects the level of the alarmone ppGpp (40) and is connected to ribosome allocation via the regulation of ribosome biogenesis by ppGpp (52, 53). For *B. subtilis*, GTP is central to the regulation of ribosome biogenesis while ppGpp is also involved by regulating GTP homeostasis (53–58). Not as much is known at the quantitative level about the elongation speed in Bs. However, the invariance of relations between the ribosome fraction and elongation rate on the scaled growth rate (Fig. 4) suggests that despite possible mechanistic differences in molecular control, these different organisms may well share the same regulatory strategy, i.e., controlling ribosome biogenesis via ribosome kinetics (ref. 40 and *SI Appendix*, *Note* S2). Very little is known about the kinetics of the ribosomes of *V. natriegens*. The fact that these ribosomes can operate so much faster than those of *E. coli* and *B. subtilis* raises the very important evolutionary question of why other organisms (including other *Vibrio* species) have not acquired such characteristics for their ribosomes.

Second, the growth rate itself can vary strongly between organisms in similar growth conditions; it is set by the maximal elongation rate of the ribosome (Eq. **1**) and is not the determinant of proteome allocation. Differences in growth rate for the same enzyme abundances imply accompanying global changes in enzyme kinetics across metabolic processes. We thus expect relations like Eq. **1** to describe the kinetics of many metabolic pathways although there are currently no known ways to measure enzyme kinetics in vivo other than those of macromolecular machineries such as the ER of the ribosome. A global increase in enzyme kinetics can arise from increase in the actual temperature (26, 39), or can be elevated in organisms like Vn through processes mimicking a temperature increase (Fig. 4 *A* and *B*) (22, 26), possibly involving changes in the cytoplasmic environment analogous to those that allow psychrophiles to remain metabolically active at low temperatures (59, 60).

Both the flexibility in enzyme kinetics (e.g., ε^*) and the rigidity in the absolute proteome allocation program (as defined by, e.g.,

ϕ^*_{tt}, $\phi^\dagger_{syn}$) are highly surprising. They are in fact the opposite of commonly held notions of evolutionary dynamics, which take the evolution of protein expression (resulting from, e.g., changes in regulatory sequences which can accumulate mutations relatively easily without disrupting protein function) as more rapid than the evolution of protein function (likely more constraining due to the functional necessity of maintaining structural integrity and biochemical properties) (61–67). These notions, arising largely from laboratory evolution experiments or comparative genomics studies of metazoan development (68–73), have been applied broadly to infer resource allocation in bacteria by optimizing growth while holding protein kinetics fixed (74–77). Our findings challenge the application of these common notions of evolvability to growing bacteria, and point to the existence of important, but currently ignored, adaptative processes shaping bacterial evolution: mechanisms that allow easy "tuning" of enzyme kinetics to allow phylogenetically similar bacteria to grow at different rates in accordance to their environments, and constraints that maintain the conservation of proteome allocation strategies for distantly related bacteria, reflecting an underlying blueprint of proteome allocation program that transcends the bacterial phylogeny.

Although the bacterial species studied here behaved similarly, our results should not be interpreted as saying that all bacterial species behave this way, i.e., there exists only one blueprint, even among the group of fast-growing chemoheterotrophs studied here. If one compares bacterial species to chemical elements, then the blueprint uncovered in this work may be analogous to an element family with similar chemical properties, e.g., the halogens or the alkali metals. Future studies of more diverse bacteria may lead to a set of such blueprints, which can help to build a "Periodic Table" of bacterial species. Such a view can provide a different perspective in the study of microbial ecology, as the "chemistry" of such interacting "elements."

Materials and Methods

See *SI Appendix, Supplementary Methods* for detailed descriptions of various experimental procedures including strain constructions, bacterial culturing procedures, measurements of RNA/protein ratio and translation elongation rates as well as quantitative proteomics analysis. For strain constructions, the IPTG-inducible *lacZ* reporter systems were established in both *B. subtilis* and *V. natriegens* for following-up measurements of translation elongation rates. The batch culturing processes contained three steps: seed culture, preculture, and final experimental culture. During the culturing process of the final experimental culture, 5 to 10 OD_{600} data points during exponential phase (generally within the OD_{600} range of 0.05 ~ 0.6) were measured by a Thermo Sci Genesys 50 spectrophotometer to obtain the growth curve and calculate the rate of exponential growth. Measurements of total RNA and protein of bacteria were the same as described in ref. 37. Measurement of translation elongation rates was based on classical LacZ induction assay (78) as implemented for *E. coli* (37) grown in different nutrient conditions. Protein abundances were measured using the 4D label-free approach on a timsTOF Pro mass spectrometry system, using the MaxQuant search engine and xTop v2.2 for protein quantification (34). Protein intensities were further length-corrected based on comparison with ribosome profiling data as described in *SI Appendix, Note* S3.

Data, Materials, and Software Availability. Raw proteomics data have been deposited into the PRIDE database (www.ebi.ac.uk/pride) as below: *B. subtilis* (both 37 °C and 43 °C): PXD057647 (79) and PXD057648 (80); *V. natriegens* (37 °C): PXD045789 (81); *E. coli* (37 °C): PXD045784 (82); *V. natriegens* and *E. coli* (30 °C): PXD057334 (83) and PXD057303 (84). All other data are included in the article and/or supporting information.

ACKNOWLEDGMENTS. We are grateful to many colleagues for helpful discussions during the course of this work, including Ross Carlson, Georg Fritz, Arvind Murugan, Elad Noor, as well as current and former members of the Hwa lab. We particularly want to acknowledge Leonardo Pacciani-Mori for sharing his knowledge and insight on the physiology of *V. natriegens* and J.T. Sauls of Suckjoon Jun's lab for sharing his unpublished data on the R-line of *B. subtilis*. We are also grateful to the two reviewers for their detailed reading of the manuscript and for their thoughtful comments which sharpened the presentation and discussion of this study. M.Z. and X.D. acknowledge support by the National Key Research and Development Program of China (2022YFF1000400), National Natural Science Foundation of China (32270034, 32370044, and 32470038), and Science Funds for Distinguished Young Scholar of Hubei Province (2022CFA044). M.M. and T.H. acknowledge support by the US NIH (Grant no. R35GM152133), the Simons Foundation through the Principles of Microbial Ecosystems (PriME) Collaboration (Grant No. 542387), and Human Frontiers in Science Program (RGP013/2024).

Author affiliations: [a]State Key Laboratory of Green Pesticides, Key Laboratory of Pesticide and Chemical Biology of Ministry of Education, Hubei Key Laboratory of Genetic Regulation and Integrative Biology, Department of Microbiology, School of Life Sciences, Central China Normal University, Wuhan 430079, China; and [b]Department of Physics, University of California, San Diego, La Jolla, CA 92093-0319

1. M. Basan, Resource allocation and metabolism: The search for governing principles. *Curr. Opin. Microbiol.* **45**, 77–83 (2018).
2. J. Kim, A. Darlington, M. Salvador, J. Utrilla, J. Jiménez, Trade-offs between gene expression, growth and phenotypic diversity in microbial populations. *Curr. Opin. Biotechnol.* **62**, 29–37 (2020).
3. N. M. Belliveau *et al.*, Fundamental limits on the rate of bacterial growth and their influence on proteomic composition. *Cell Syst.* **12**, 924–944.e922 (2021).
4. M. Scott, T. Hwa, Shaping bacterial gene expression by physiological and proteome allocation constraints. *Nat. Rev. Microbiol.* **21**, 327–342 (2023).
5. C. Liao, P. Priyanka, Y. H. Lai, C. V. Rao, T. Lu, How does *Escherichia coli* allocate proteome? *ACS Synth Biol.* **13**, 2718–2732 (2024).
6. K. Zengler, B. O. Palsson, A road map for the development of community systems (CoSy) biology. *Nat. Rev. Microbiol.* **10**, 366–372 (2012).
7. S. Mitri, K. R. Foster, The genotypic view of social interactions in microbial communities. *Annu. Rev. Genet.* **47**, 247–273 (2013).
8. E. A. Franzosa *et al.*, Sequencing and beyond: Integrating molecular "omics" for microbial community profiling. *Nat. Rev. Microbiol.* **13**, 360–372 (2015).
9. K. Zengler, L. S. Zaramela, The social network of microorganisms - how auxotrophies shape complex communities. *Nat. Rev. Microbiol.* **16**, 383–390 (2018).
10. S. Li, S. Muller, Ecological forces dictate microbial community assembly processes in bioreactor systems. *Curr. Opin. Biotechnol.* **81**, 102917 (2023).
11. D. P. Smith *et al.*, Proteomic and transcriptomic analyses of "Candidatus Pelagibacter ubique" describe the first PII-independent response to nitrogen limitation in a free-living Alphaproteobacterium. *mBio* **4**, e00133-00112 (2013).
12. A. Schmidt *et al.*, The quantitative and condition-dependent Escherichia coli proteome. *Nat. Biotechnol.* **34**, 104–110 (2016).
13. J. B. Lalanne *et al.*, Evolutionary convergence of pathway-specific enzyme expression stoichiometry. *Cell* **173**, 749–761.e738 (2018).
14. T. Zavel *et al.*, Quantitative insights into the cyanobacterial cell economy. *eLife* **8**, e42508 (2019).
15. A. L. Müller *et al.*, An alternative resource allocation strategy in the chemolithoautotrophic archaeon *Methanococcus maripaludis*. *Proc. Natl. Acad. Sci. U.S.A.* **118**, e2025854118 (2021).
16. M. Mori *et al.*, From coarse to fine: The absolute *Escherichia coli* proteome under diverse growth conditions. *Mol. Syst. Biol.* **17**, e9536 (2021).
17. G. W. Li, D. Burkhardt, C. Gross, J. S. Weissman, Quantifying absolute protein synthesis rates reveals principles underlying allocation of cellular resources. *Cell* **157**, 624–635 (2014).
18. K. Peebo *et al.*, Proteome reallocation in *Escherichia coli* with increasing specific growth rate. *Mol. Biosyst.* **11**, 1184–1193 (2015).
19. A. Mateus *et al.*, The functional proteome landscape of *Escherichia coli*. *Nature* **588**, 473–478 (2020).
20. D. A. Ratkowsky, J. Olley, T. A. McMeekin, A. Ball, Relationship between temperature and growth rate of bacterial cultures. *J. Bacteriol.* **149**, 1–5 (1982).
21. S. Vieira-Silva, E. P. Rocha, The systemic imprint of growth and its uses in ecological (meta)genomics. *PLoS Genet.* **6**, e1000808 (2010).
22. V. L. Arcus *et al.*, On the temperature dependence of enzyme-catalyzed rates. *Biochemistry* **55**, 1681–1688 (2016).
23. B. R. K. Roller, S. F. Stoddard, T. M. Schmidt, Exploiting rRNA operon copy number to investigate bacterial reproductive strategies. *Nat. Microbiol.* **1**, 16160 (2016).
24. J. L. Weissman, S. Hou, J. A. Fuhrman, Estimating maximal microbial growth rates from cultures, metagenomes, and single cells via codon usage patterns. *Proc. Natl. Acad. Sci. U.S.A.* **118**, e2016810118 (2021).
25. F. Mairet, J. L. Gouzé, H. de Jong, Optimal proteome allocation and the temperature dependence of microbial growth laws. *NPJ Syst. Biol. Appl.* **7**, 14 (2021).
26. B. D. Knapp, K. C. Huang, The effects of temperature on cellular physiology. *Annu. Rev. Biophys.* **51**, 499–526 (2022).
27. O. Cohen *et al.*, Comparative transcriptomics across the prokaryotic tree of life. *Nucleic Acids Res.* **44**, W46–53 (2016).

28. E. I. Tocheva, D. R. Ortega, G. J. Jensen, Sporulation, bacterial cell envelopes and the origin of life. *Nat. Rev. Microbiol.* **14**, 535–542 (2016).
29. M. T. Weinstock, E. D. Hesek, C. M. Wilson, D. G. Gibson, *Vibrio natriegens* as a fast-growing host for molecular biology. *Nat. Methods* **13**, 849–851 (2016).
30. H. H. Lee *et al.*, Functional genomics of the rapidly replicating bacterium *Vibrio natriegens* by CRISPRi. *Nat. Microbiol.* **4**, 1105–1113 (2019).
31. O. Maaløe, "Regulation of the protein-synthesizing machinery – ribosomes, tRNA, factors, and so on" in *Biological Regulation and Development*, R. F. Goldberger, Ed. (Plenum, New York, NY, 1979).
32. M. Scott, C. W. Gunderson, E. M. Mateescu, Z. Zhang, T. Hwa, Interdependence of cell growth and gene expression: Origins and consequences. *Science* **330**, 1099–1102 (2010).
33. A. G. Planson, V. Sauveplane, E. Dervyn, M. Jules, Bacterial growth physiology and RNA metabolism. *Biochim. Biophys. Acta Gene Regul. Mech.* **1863**, 194502 (2020).
34. C. Wu *et al.*, Enzyme expression kinetics by *Escherichia coli* during transition from rich to minimal media depends on proteome reserves. *Nat. Microbiol.* **8**, 347–359 (2023).
35. J. Hoff *et al.*, Vibrio natriegens: An ultrafast-growing marine bacterium as emerging synthetic biology chassis. *Environ. Microbiol.* **22**, 4394–4408 (2020).
36. J. Xu, S. Yang, L. Yang, Vibrio natriegens as a host for rapid biotechnology. *Trends Biotechnol.* **40**, 381–384 (2022).
37. X. Dai *et al.*, Reduction of translating ribosomes enables *Escherichia coli* to maintain elongation rates during slow growth. *Nat. Microbiol.* **2**, 16231 (2016).
38. H. Bremer, P. P. Dennis, Modulation of chemical composition and other parameters of the cell at different exponential growth rates. *EcoSal Plus* **3**, 1–48 (2008).
39. A. Farewell, F. C. Neidhardt, Effect of temperature on in vivo protein synthetic capacity in *Escherichia coli*. *J. Bacteriol.* **180**, 4704–4710 (1998).
40. C. Wu *et al.*, Cellular perception of growth rate and the mechanistic origin of bacterial growth law. *Proc. Natl. Acad. Sci. U.S.A.* **119**, e2201585119 (2022).
41. J. Qiao *et al.*, Research advances in the identification of regulatory mechanisms of surfactin production by Bacillus: A review. *Microb Cell Fact* **23**, 100 (2024).
42. C. S. Barker, B. M. Prüss, P. Matsumura, Increased motility of *Escherichia coli* by insertion sequence element integration into the regulatory region of the flhD operon. *J. Bacteriol.* **186**, 7529–7537 (2004).
43. K. A. Fahrner, H. C. Berg, Mutations that stimulate flhDC expression in *Escherichia coli* K-12. *J. Bacteriol.* **197**, 3087–3096 (2015).
44. Z. Zhang, C. Kukita, M. Z. Humayun, M. H. Saier, Environment-directed activation of the Escherichia coliflhDC operon by transposons. *Microbiology (Reading)* **163**, 554–569 (2017).
45. R. Allard-Massicotte *et al.*, *Bacillus subtilis* early colonization of *Arabidopsis* thaliana roots involves multiple chemotaxis receptors. *mBio* **7**, e01664 (2016).
46. A. Levy *et al.*, Genomic features of bacterial adaptation to plants. *Nat. Genet* **50**, 138–150 (2017).
47. T. Tian *et al.*, Sucrose triggers a novel signaling cascade promoting Bacillus subtilis rhizosphere colonization. *ISME J.* **15**, 2723–2737 (2021).
48. D. R. Zeigler *et al.*, The origins of 168, W23, and other *Bacillus subtilis* legacy strains. *J. Bacteriol.* **190**, 6983–6995 (2008).
49. H. Tettelin, D. Riley, C. Cattuto, D. Medini, Comparative genomics: The bacterial pan-genome. *Curr. Opin. Microbiol.* **11**, 472–477 (2008).
50. G. Vernikos, D. Medini, D. R. Riley, H. Tettelin, Ten years of pan-genome analyses. *Curr. Opin. Microbiol.* **23**, 148–154 (2015).
51. A. A. Golicz, P. E. Bayer, P. L. Bhalla, J. Batley, D. Edwards, Pangenomics comes of age: From bacteria to plant and animal applications. *Trends Genet.* **36**, 132–145 (2020).
52. K. Potrykus, M. Cashel, p)ppGpp: Still magical? *Annu. Rev. Microbiol.* **62**, 35–51 (2008).
53. R. L. Gourse *et al.*, Transcriptional responses to ppGpp and DksA. *Annu. Rev. Microbiol.* **72**, 163–184 (2018).
54. L. Krásný, R. L. Gourse, An alternative strategy for bacterial ribosome synthesis: *Bacillus subtilis* rRNA transcription regulation. *Embo J.* **23**, 4473–4483 (2004).
55. A. Kriel *et al.*, Direct regulation of GTP homeostasis by (p)ppGpp: A critical component of viability and stress resistance. *Mol. Cell* **48**, 231–241 (2012).
56. A. Kriel *et al.*, GTP dysregulation in *Bacillus subtilis* cells lacking (p)ppGpp results in phenotypic amino acid auxotrophy and failure to adapt to nutrient downshift and regulate biosynthesis genes. *J. Bacteriol.* **196**, 189–201 (2014).
57. A. N. Bittner, A. Kriel, J. D. Wang, Lowering GTP level increases survival of amino acid starvation but slows growth rate for Bacillus subtilis cells lacking (p)ppGpp. *J. Bacteriol.* **196**, 2067–2076 (2014).
58. R. Thiermann, "Resource allocation and growth rate control in bacteria," PhD thesis, UC San Diego (2024).
59. G. N. Somero, Adaptation of enzymes to temperature: Searching for basic "strategies". *Comp. Biochem. Physiol. B Biochem. Mol. Biol.* **139**, 321–333 (2004).
60. P. H. Yancey, Organic osmolytes as compatible, metabolic and counteracting cytoprotectants in high osmolarity and other stresses. *J. Exp. Biol.* **208**, 2819–2830 (2005).
61. R. J. Britten, E. H. Davidson, Gene regulation for higher cells: A theory. *Science* **165**, 349–357 (1969).
62. E. H. Davidson, *Genomic Regulatory Systems* (Academic Press, San Diego, CA, 2001).
63. J. W. Valentine, *On The Origin of Phyla* (University of Chicago Press, Chicago, IL, 2004).
64. S. B. Carroll, J. K. Grenier, S. D. Weatherbee, *From DNA to Diversity, Molecular Genetics and the Evolution of Animal Design*. (Wiley-Blackwell, Ed.2, 2004).
65. M. Lynch, The evolution of genetic networks by non-adaptive processes. *Nat. Rev. Genet.* **8**, 803–813 (2007).
66. B. Prud'homme, N. Gompel, S. B. Carroll, Emerging principles of regulatory evolution. *Proc. Natl. Acad. Sci. U.S.A.* **104**, 8605–8612 (2007).
67. G. A. Wray, The evolutionary significance of cis-regulatory mutations. *Nat. Rev. Genet.* **8**, 206–216 (2007).
68. D. M. Weinreich, N. F. Delaney, M. A. Depristo, D. L. Hartl, Darwinian evolution can follow only very few mutational paths to fitter proteins. *Science* **312**, 111–114 (2006).
69. N. Philippe, E. Crozat, R. E. Lenski, D. Schneider, Evolution of global regulatory networks during a long-term experiment with *Escherichia coli*. *Bioessays* **29**, 846–860 (2007).
70. S. B. Carroll, Evo-devo and an expanding evolutionary synthesis: A genetic theory of morphological evolution. *Cell* **134**, 25–36 (2008).
71. D. L. Stern, V. Orgogozo, The loci of evolution: How predictable is genetic evolution? *Evolution* **62**, 2155–2177 (2008).
72. M. Barkoulas, A. M. Vargas Velazquez, A. E. Peluffo, M. A. Félix, Evolution of new cis-regulatory motifs required for cell-specific gene expression in caenorhabditis. *PLoS Genet.* **12**, e1006278 (2016).
73. R. C. Lin, B. T. Ferreira, Y. W. Yuan, The molecular basis of phenotypic evolution: Beyond the usual suspects. *Trends Genet.* **40**, 668–680 (2024).
74. D. Molenaar, R. van Berlo, D. de Ridder, B. Teusink, Shifts in growth strategies reflect tradeoffs in cellular economics. *Mol. Syst. Biol.* **5**, 323 (2009).
75. E. J. O'Brien, J. A. Lerman, R. L. Chang, D. R. Hyduke, B. Palsson, Genome-scale models of metabolism and gene expression extend and refine growth phenotype prediction. *Mol. Syst. Biol.* **9**, 693 (2013).
76. F. J. Bruggeman, R. Planque, D. Molenaar, B. Teusink, Searching for principles of microbial physiology. *FEMS Microbiol. Rev.* **44**, 821–844 (2020).
77. H. Dourado, M. J. Lercher, An analytical theory of balanced cellular growth. *Nat. Commun.* **11**, 1226 (2020).
78. R. Schleif, W. Hess, S. Finkelstein, D. Ellis, Induction kinetics of the L-arabinose operon of *Escherichia coli*. *J. Bacteriol.* **115**, 9–14 (1973).
79. M. Zhu, X. Dai, Data from "*B. subtilis* proteome." PRIDE. https://www.ebi.ac.uk/pride/archive/projects/PXD057647. Accessed 11 August 2024.
80. M. Zhu, X. Dai, Data from "*Bacillus subtilis* proteome." PRIDE. https://www.ebi.ac.uk/pride/archive/projects/PXD057648. Accessed 11 August 2024.
81. M. Zhu, X. Dai, Data from "*V. natriegens* proteome under nutrient limitation." PRIDE. https://www.ebi.ac.uk/pride/archive/projects/PXD045789. Accessed 28 September 2023.
82. M. Zhu, X. Dai, Data from "*E. coli* proteome under nutrient limitation." PRIDE. https://www.ebi.ac.uk/pride/archive/projects/PXD045784. Accessed 28 September 2023.
83. M. Zhu, X. Dai, Data from "*V. natriegens* proteome under nutrient limitation." PRIDE. https://www.ebi.ac.uk/pride/archive/projects/PXD057334. Accessed 30 October 2024.
84. M. Zhu, X. Dai, Data from "*E. coli* proteome under nutrient limitation." PRIDE. https://www.ebi.ac.uk/pride/archive/projects/PXD057303. Accessed 29 October 2024.